Supporting Information

(10 pages, 6 figures)

Assessment of long-term performance and chromate reduction mechanisms in a field scale permeable reactive barrier

BETTINA FLURY[†], JAKOB FROMMER[‡], URS EGGENBERGER[†], URS MÄDER[†,*], MAARTEN NACHTEGAAL [§], RUBEN KRETZSCHMAR [‡]

Rock-Water Interaction Group, Institute of Geological Sciences, University of Bern, Switzerland, Institute of Biogeochemistry and Pollutant Dynamics, Department of Environmental Sciences, ETH Zürich, Switzerland, and Paul Scherrer Institute, General Energy Research Department, Laboratory for Energy and Materials Cycles, Villigen, Switzerland

Environmental Science and Technology

Prepared: May 11, 2009

---

[*] Corresponding author

[†] University of Bern

[‡] ETH Zürich

[§] Paul Scherrer Institute

1. Preparation of reference material, metal speciation, mineralogical characterization, and microbiological analysis

Reference samples

Goethite and (2-line)-ferrihydrite were synthesized according to published methods (1). A natural siderite specimen was obtained from the mineral-collection of the ETH Zurich (Dr. P. Brack). Magnetite was isolated from a granite sample (M. Kiczka, ETH Zürich). The Cr-Fe-hydroxides were synthesized following a published method (2) which was slightly modified. In short, the synthesis involved the titration of appropriate mixtures of $Cr(NO_3)_3 \cdot 9H_2O$ and $Fe(NO_3)_3 \cdot 9H_2O$ (0.2M) with NaOH to pH 7. This pH was maintained for 2d. Subsequently the product was washed twice with high purity (18 MΩcm) water and freeze dried. The Cr/Fe ratio was verified by XRF analysis (± 3 mole%).

Instrumentation and data analysis for bench-top μ-XRF, synchrotron μ-XRF and μ-XAFS analyses

Thin-section-samples were analyzed in fluorescence mode and were mounted at 45° to the incident beam. Fluorescent intensities were normalized to the incident intensity (measured by an ionization chamber (Advanced Light Source (ALS), Berkeley, USA)) or a diode (Swiss Light Source (SLS), Villigen, CH). Element distribution maps were obtained at incident photon energies of 10 keV and (occasionally) at 5 keV (for light elements). The beamsize was generally $2\times2\mu m^2$ (SLS) or between 5×5 and 7×7 μm^2 (ALS), respectively. Evaluation of the synchrotron-based μ-XRF mapping-data was done by software developed at ALS beamline 10.3.2 (3). For all element maps shown the black-level is set to 0 counts while the white-level was set to the 99^{th} percentile (i.e. 99% of the pixels have an intensity of smaller or equal to the selected value).

Mapping of Cr in ZVI-shavings not installed into the barrier (data not shown) did indicate a heterogeneous but stochastic distribution of Cr contained in pristine ZVI-shavings (0.05-0.4%). Interferences with the metal speciation in the corrosion crust are not expected.

At selected points of interest (POI) Fe K-edge or Cr K-edge μ-XANES spectra were recorded. The single scans were aligned by using the monochromator-glitches at 5986.1eV (Cr) and 7265eV (Fe), respectively (ALS). Due to the high Fe concentration in the sample the Fe spectra were distorted by the "over-absorption" effect (4). Efforts to mitigate this effect by using a grazing exit detection scheme were unsuccessful presumably due to the intrinsic surface roughness. Using the spectra of goethite, siderite (measured at ALS), 2-line-ferrihydrite and magnetite (measured at HASYLAB with a similar experimental broadening) the Fe-μ-XANES spectra were analyzed by linear combination fitting (LCF) using the software code ATHENA (5). A factor correcting for self-absorption was included into the fitting procedure for some spectra (software developed at the ALS beamline 10.3.2). The fractions were optimized by minimizing the normalized sum-square error (i.e. squares of the residuals divided by the squares of the data). Given the complexity of the samples and the occurrence of over-absorption artifacts no well-defined solutions were expected. The Fe(II)/Fe(III) ratio was, however, rather stable even though the fractions of the single Fe(III) (hydr)oxides did vary depending on the parameter chosen (self-absorption, number of references in the fit) without having a pronounced effect on the goodness of the fit. The quantitative Fe speciation is therefore connected to uncertainties (estimated to be in the order of 10-20% (absolute)) (6).

Bulk Cr K-edge XANES spectra were collected at beamline A1 of the Hamburger Synchrotronstrahlungslabor (HASYLAB, Hamburg, Germany) using a Si(111) DCM (detuned to 60% using a software-controlled monochromator stabilization). The reference samples were pressed into pellets (diluents: boron carbide and Licowax C®) and measured in transmission (using N_2 filled ionization chambers). Comparing spectra measured at ALS and at HASYLAB (not shown) suggest a similar experimental broadening for both lines, but no efforts have been made to quantify this effect.

Extraction of XANES from the raw data has been done following standard methods and using the software code ATHENA (5).

Beam damage

It has been reported that the speciation in environmental samples may change during sample preparation and upon irradiation with energetic photons. Cr(III) expected to result from chromate reduction within the barrier, is however much less susceptible to beam-induced changes than chromate. We did not observe any changes in the XAFS spectra over time.

Sample preparation and instrumentation for XRD and Raman spectroscopy

Samples were acetone dried under vacuum and the iron shavings were separated from the gravel for analyses. For X-ray diffraction analysis, the shavings were scraped off and finely ground. For Raman spectroscopy, the iron shavings were embedded in a two-component epoxy resin (Epotex, Polyscience AG) and prepared as polished microsections (3-5 mm thick).

For powder XRD an X'Pert Pro, Panalytical with a Cu Kα radiation and an X'Celerator detector were used. Measurement conditions were 40 kV and 40 mA over the range of 5-120 °2Theta with 20 sec/step. The Raman analyses were conducted on a Jobin Yvon LabRAM-HR800 instrument consisting of an Olympus BX41 confocal microscope coupled to an 800 mm focal-length spectrograph. Measurements were performed using a He/Ne laser with an excitation wavelength of 632.817 nm (red) and a sample power of about 19 mW. Acquisition time for most measurements was 2x120s.

Characterization of the organic material

Sampling of organic matter occurred in June 2006. The organic film was scraped off from the surface of the MPSS by a spatula and immediately fixed on a small glass plate with glutaraldehyde solution (Merck, 25 %) to preserve specimens for microscopic analyses.

2. Additional data

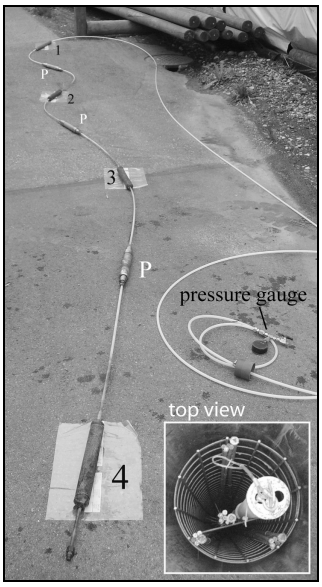

Figure S1: Multi-port sampling system (MPSS). The reactive material for sampling was placed within wire-mesh cages (1-4). The packers (P) prevent a vertical flow and hold the cages in place. Number 1 (top) to 4 (bottom) represent levels of depths (level 1: 13.0-14.0 m; level 2: 15.6-16.0 m; level 3: 18.1-19.1 m; level 4: 20.7-21.7 m). Top view shows installation within the pile: bundles of small tubes serve for sampling reactive material (2″-piezometers) and groundwater (1″-piezometers). The single large tube and the steel rod frame are for fixation.

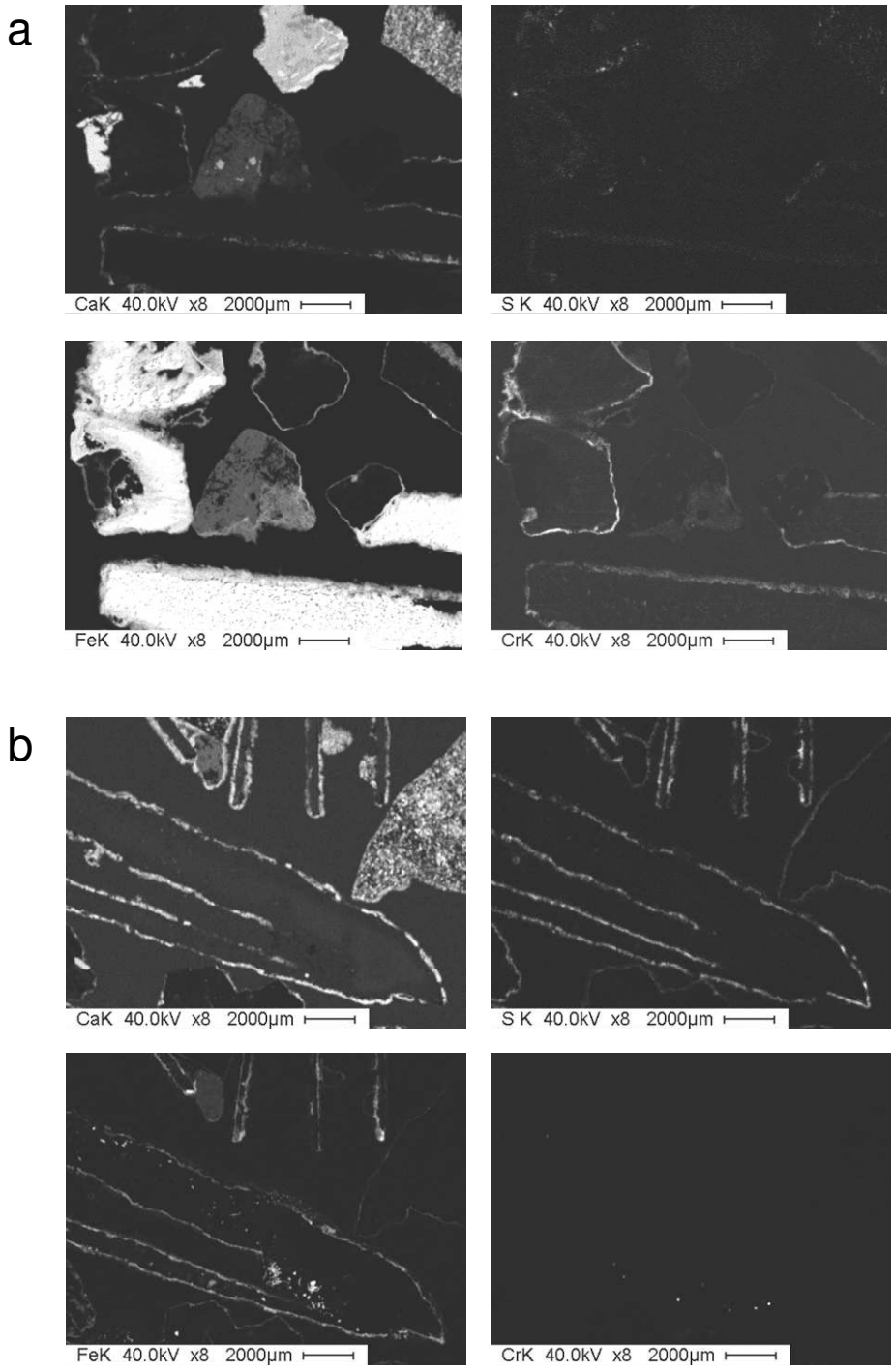

Figure S2: µ-XRF (µ-eagle) distribution maps of Ca, S, Fe, and Cr. (a) Fe shaving and gravel (Ca within the particle) sampled in the inflow of the front cylinder (A1 level2): Cr is mainly enriched around the metal particle but also (to a much lesser extend) around the gravel; only weak and isolated S enrichments. (b) Material sampled at lower level in the centre of the same pile (A2 level 3): the bulk of the ZVI particle was lost during sample preparation, thus only the crust is seen. Less secondary Fe containing precipitates are formed on the

Ca particle (in addition the weak Fe counts around the Ca-rich gravel particle correlate with S); only very weak and sporadic Cr counts.

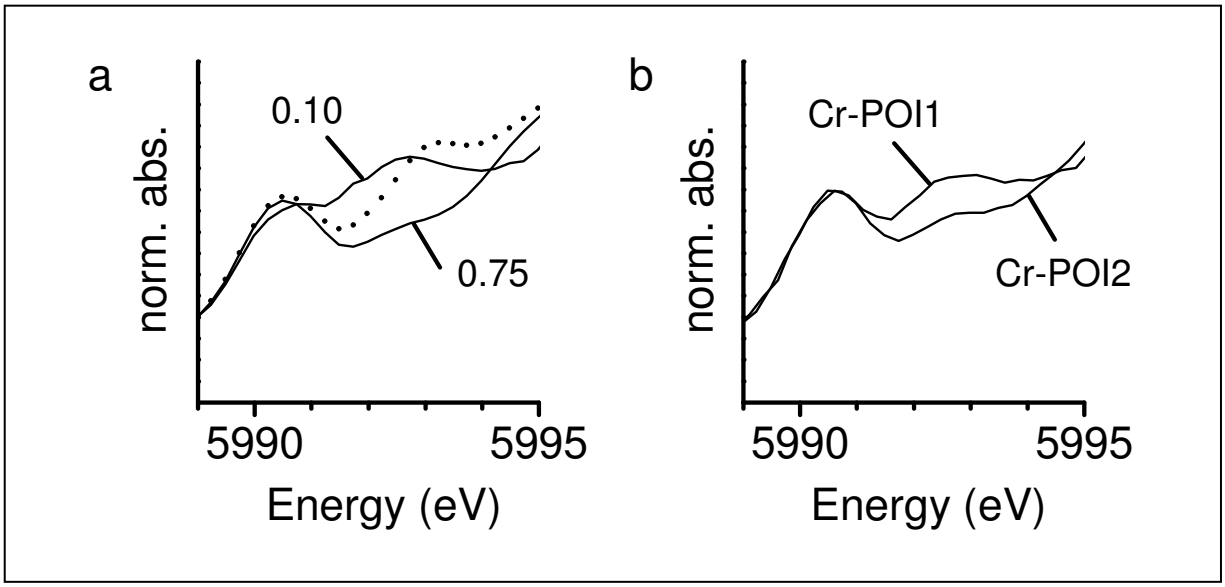

Figure S3: (a) enlarged view of the pre-edge spectra of the two end-members of the CrIII-FeIII-hydroxide series. The dotted line is the linear combination of 0.98*75-mole%-Cr-hydroxide and of 0.02*K2Cr2O7 and shows that the pre-peak of the 10-mole%-Cr-sample is not due to CrVI. (b) enlarged view of the pre-edge spectra of Cr-POI1 and Cr-POI2.

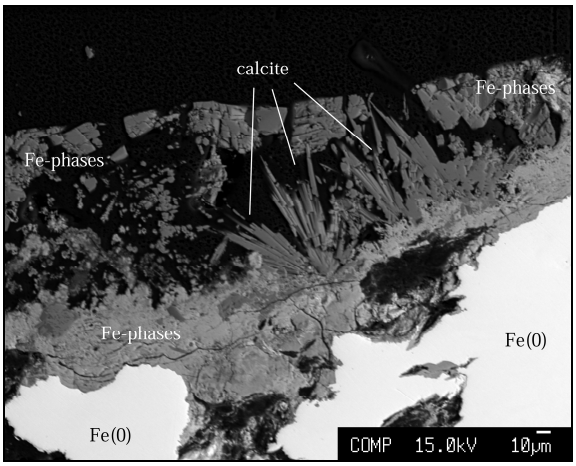

Figure S4: SEM picture of a corrosion rind of an iron shaving. Beside Fe-phases (mainly Fe^{III}-hydroxides) newly formed calcite crystals can be seen in the shape of needles. White areas represent the metallic iron (Fe0) and grey areas the corrosion rind. The epoxy resin appears in black.

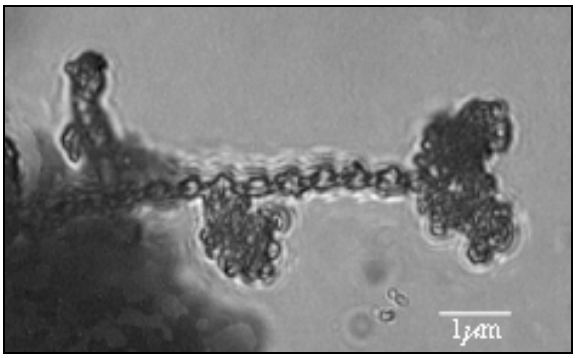

Figure S5: Optical microscope image of red slime mainly containing mainly organic matter. The iron oxidizing bacteria *gallionella ferruginea* is identified by the double helix structure. These chemolithotrophic bacteria prefer to live in neutral to slightly oxidizing environments with a redox potential around 170 mV and a content of dissolved oxygen of 0.1-1 mg/l. They oxidize ferrous iron and produce insoluble precipitates of ferric hydroxides (7).

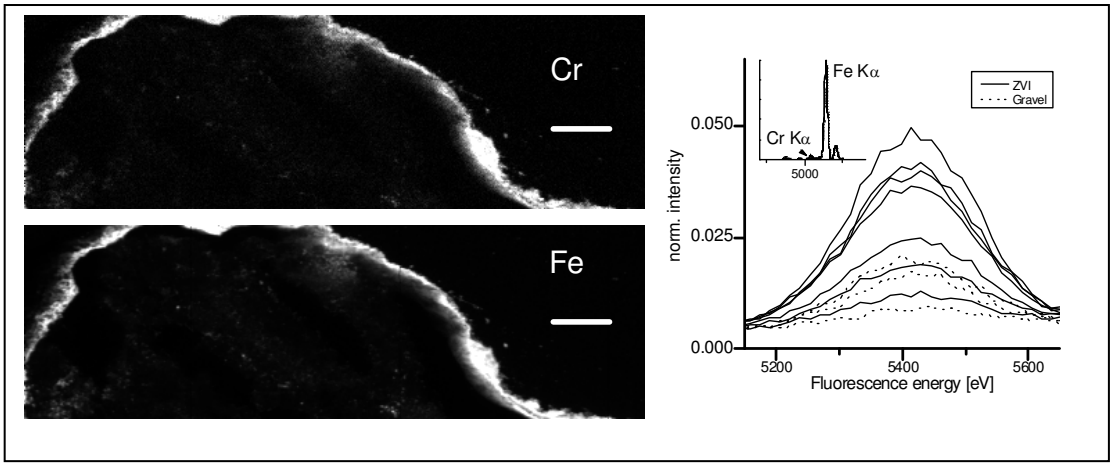

Figure S6: Precipitate crust formed on a gravel particle (high Ca and P signal) sampled at the inflow of the front-pile (A1; level 2). Left: synchrotron μ-XRF map (Scalebar = 200um). Right: Intensity of the Cr-Kα fluorescence line (normalized to the intensity of the Fe-Kα-line) measured with the same settings in the precipitate crust of the gravel particle and in the corrosion crust of a ZVI particle (the upper 4 lines were Cr hotspots while the remaining lines are measured in the matrix of the crust). The inset shows Fe Kα and Cr Kα.

3. Literature cited

(1) Schwertmann, U.; Cornell, R. M. *Iron oxides in the laboratory. Preparation and characterization*; WILEY-VCH, 2000.

(2) Hansel, C. M.; Wielinga, B. W.; Fendorf, S. R. Structural and compositional evolution of Cr/Fe solids after indirect chromate reduction by dissimilatory iron-reducing bacteria. *Geochim. Cosmochim. Acta* **2003**, *67*, 401-412.

(3) Manceau, A.; Marcus, M. A.; Tamura, N. Quantitative speciation of heavy metals in soils and sediments by synchrotron X-ray techniques. In *Applications of synchrotron radiation in low-temperature geochemistry and environmental science.*; Sturchio, N. C., Fenter, P., Sutton, S. R., Rivers, M. L., Eds.; Mineralogical Society of America: Washington, D.C., 2002; pp 341-428.

(4) Grolimund, D.; Senn, M.; Trottmann, M.; Janousch, M.; Bonhoure, I.; Scheidegger, A. M.; Marcus, M. Shedding new light on historical metal samples using micro-focused synchrotron X-ray fluorescence and spectroscopy. *Spectrochim. Acta* **2004**, *59*, 1627-1635.

(5) Ravel, B.; Newville, M. ATHENA; ARTEMIS; HEPHAESTUS: data analysis for X-ray absorption spectroscopy using IFEFFIT. *J. Synchr. Rad.* **2005**.

(6) O'Day, P. A.; Rivera, J. N.; Root, R.; Carroll, S. A. X-ray absorption spectroscopic study of Fe reference compounds for the analysis of natural sediments. *Am. Mineral.* **2004**, *89*, 572-585.

(7) Anderson, C. R.; Pedersen, K. *In situ* growth of *Gallionella* biofilms and partitioning of lanthanides and actinides between biological material and ferric oxyhydroxides. *Geobiology* **2003**, 169-178.